Supplement of Geosci. Model Dev., 16, 6413–6431, 2023
https://doi.org/10.5194/gmd-16-6413-2023-supplement

Geoscientific Model Development
Open Access
EGU

Supplement of

Implementation of a satellite-based tool for the quantification of CH_4 emissions over Europe (AUMIA v1.0) – Part 1: forward modelling evaluation against near-surface and satellite data

Angel Liduvino Vara-Vela et al.

Correspondence to: Angel Liduvino Vara-Vela (angel@geo.au.dk)

Supplement

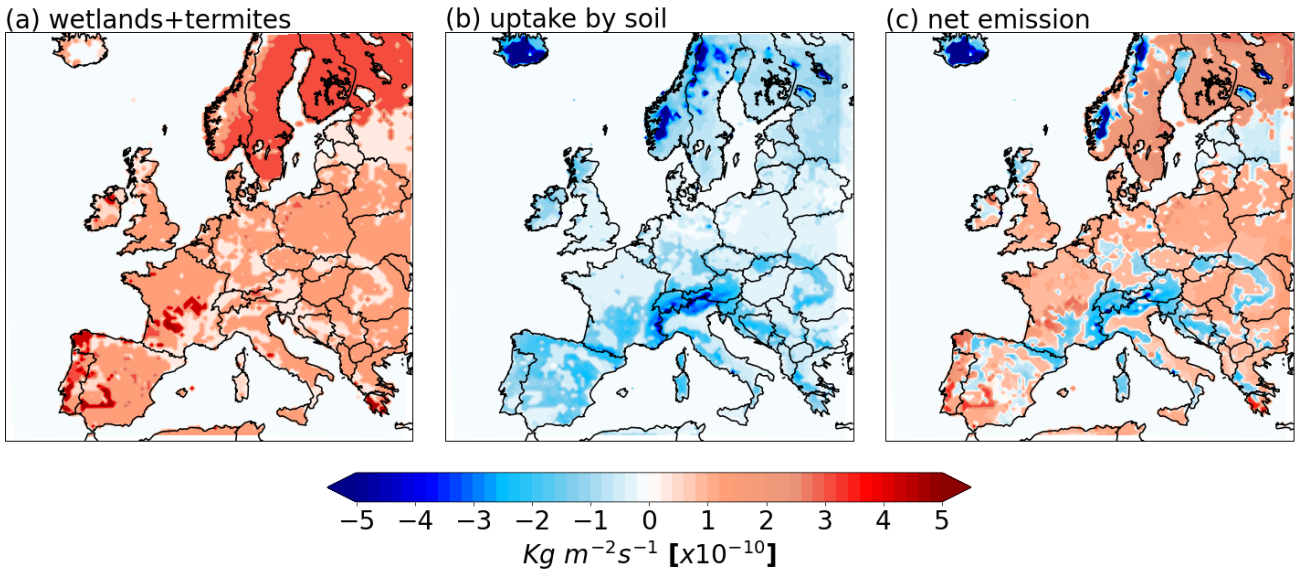

Figure S1. Temporal mean spatial distribution of CH_4 emission rate for natural sources (wetlands and termites) and sinks (soil uptake) in the 30 km modeling domain, averaged over the period from May 1 to 31, 2018..

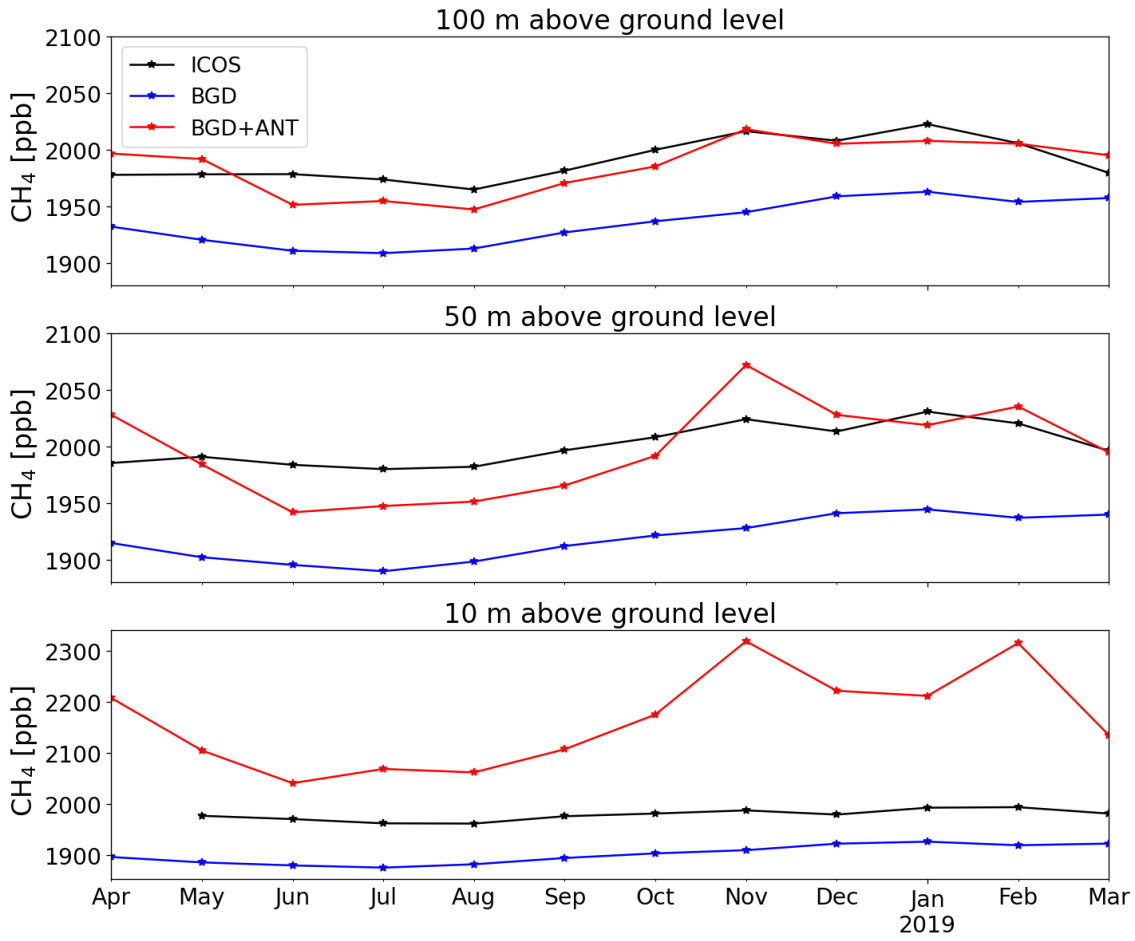

Figure S2. Monthly mean concentrations of observed (ICOS) and simulated (BGD and BGD+ANT) CH_4 at 10, 50 and 100 m above ground level for all stations. BGD and ANT represent the simulated concentrations from background and anthropogenic sources, respectively. The mean concentrations were computed based on quality-controlled ICOS CH_4 data. Contributions from natural sources (wetlands and termites) and biomass burning were not relevant during the study period.

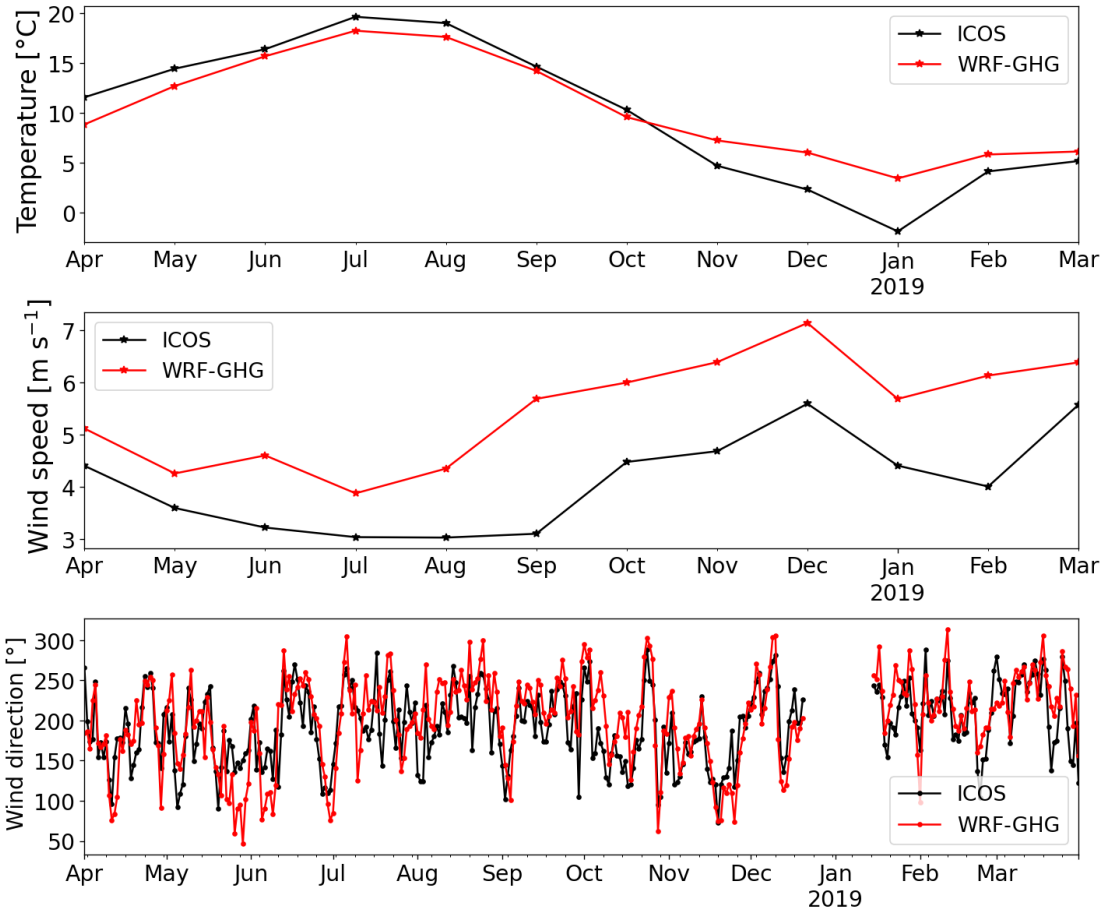

Figure S3. Monthly (and daily) mean values of observed and simulated temperature, wind speed (and wind direction) at 10 m above ground level. The mean concentrations were computed based on quality-controlled ICOS data.

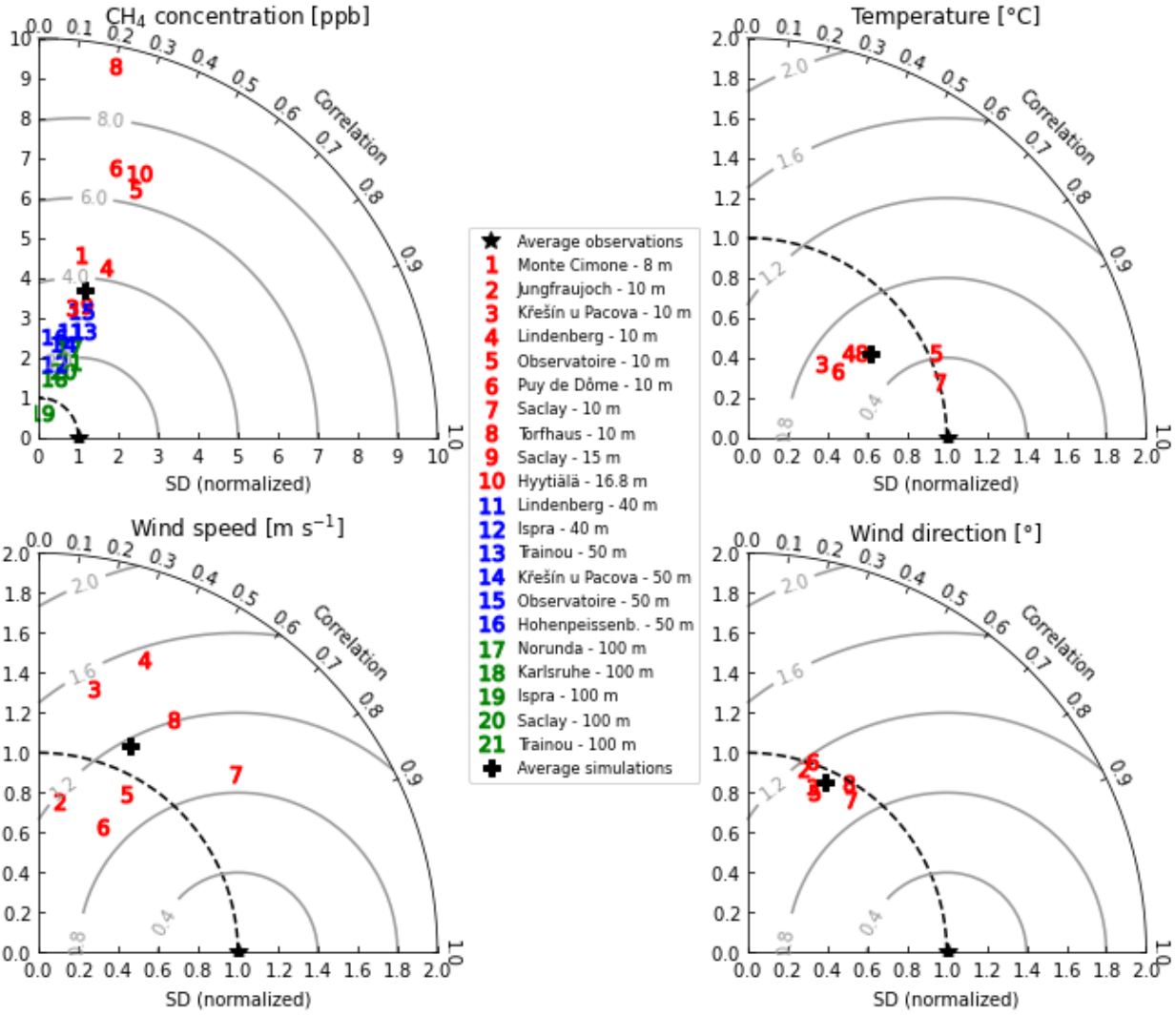

Figure S4. Correlation coefficients and standard deviation (SD) model to observation ratios for CH_4 concentrations, temperature, wind speed and wind direction. The numbers in red, blue and green represent ICOS stations with data with sampling heights between 8.0–16.8 m, 40–50 m, and 100 m, respectively (see Table 3 for station details).

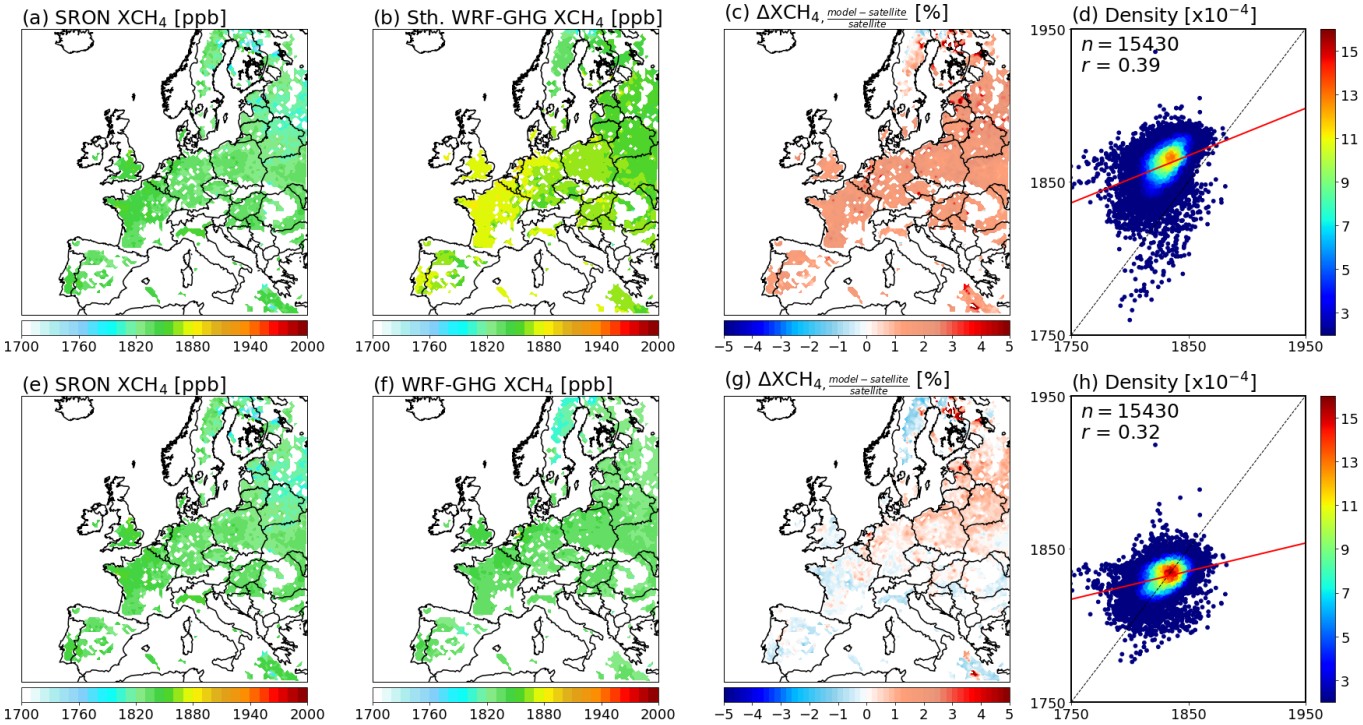

Figure S5. Temporal mean spatial distributions of XCH_4 concentration from SRON RemoTeC-S5P (panels a and e) and WRF-GHG estimates with and without smoothing (panels b and f, respectively), along with their relative differences (panels c and g), averaged over the period from April 1 to April 30, 2018.

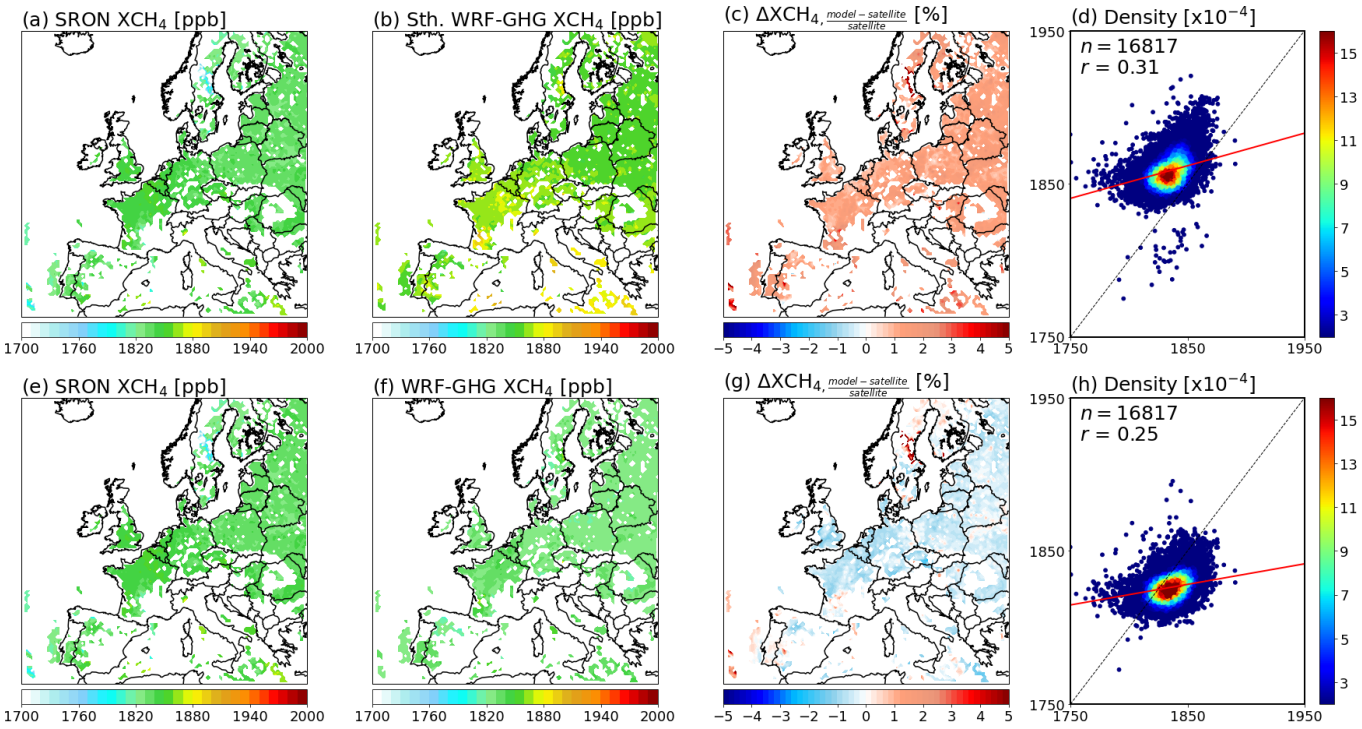

Figure S6. Temporal mean spatial distributions of XCH_4 concentration from SRON RemoTeC-S5P (panels a and e) and WRF-GHG estimates with and without smoothing (panels b and f, respectively), along with their relative differences (panels c and g), averaged over the period from May 1 to May 31, 2018.

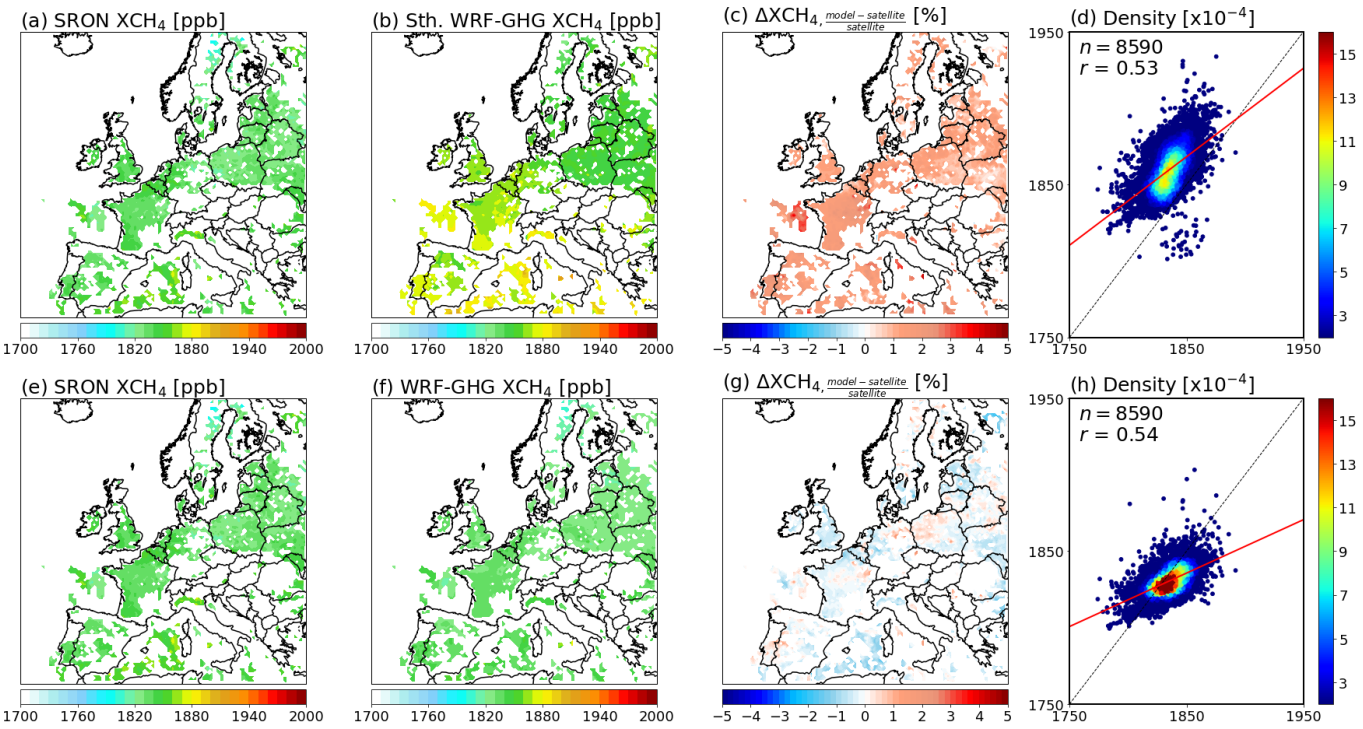

Figure S7. Temporal mean spatial distributions of XCH_4 concentration from SRON RemoTeC-S5P (panels a and e) and WRF-GHG estimates with and without smoothing (panels b and f, respectively), along with their relative differences (panels c and g), averaged over the period from June 1 to June 30, 2018.

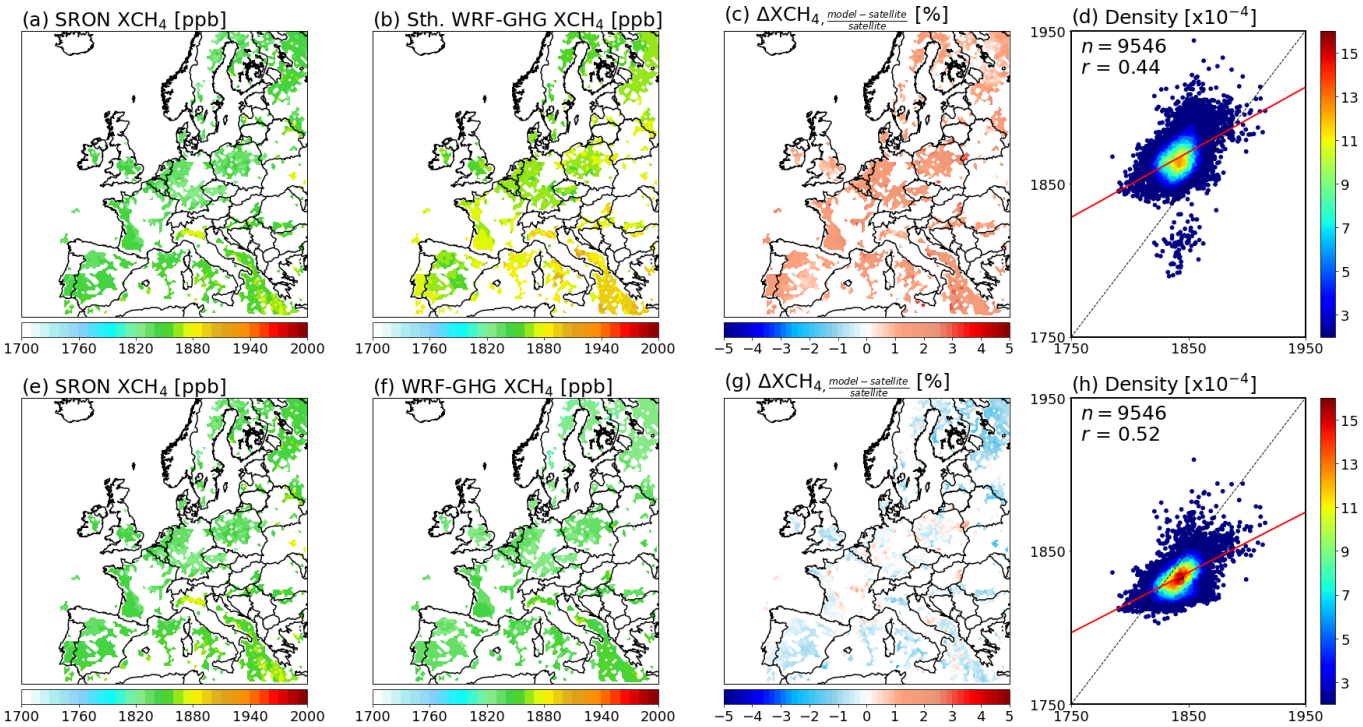

Figure S8. Temporal mean spatial distributions of XCH_4 concentration from SRON RemoTeC-S5P (panels a and e) and WRF-GHG estimates with and without smoothing (panels b and f, respectively), along with their relative differences (panels c and g), averaged over the period from July 1 to July 31, 2018.

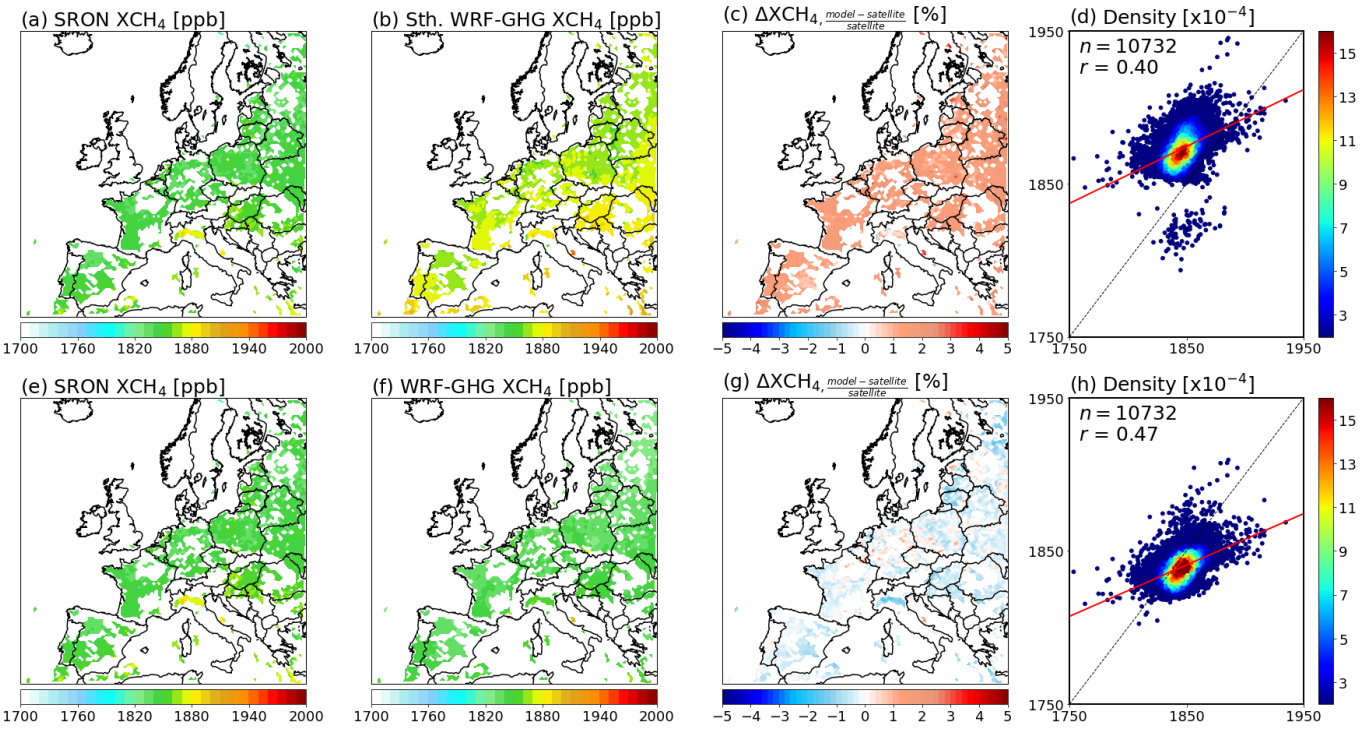

Figure S9. Temporal mean spatial distributions of XCH_4 concentration from SRON RemoTeC-S5P (panels a and e) and WRF-GHG estimates with and without smoothing (panels b and f, respectively), along with their relative differences (panels c and g), averaged over the period from August 1 to August 31, 2018.

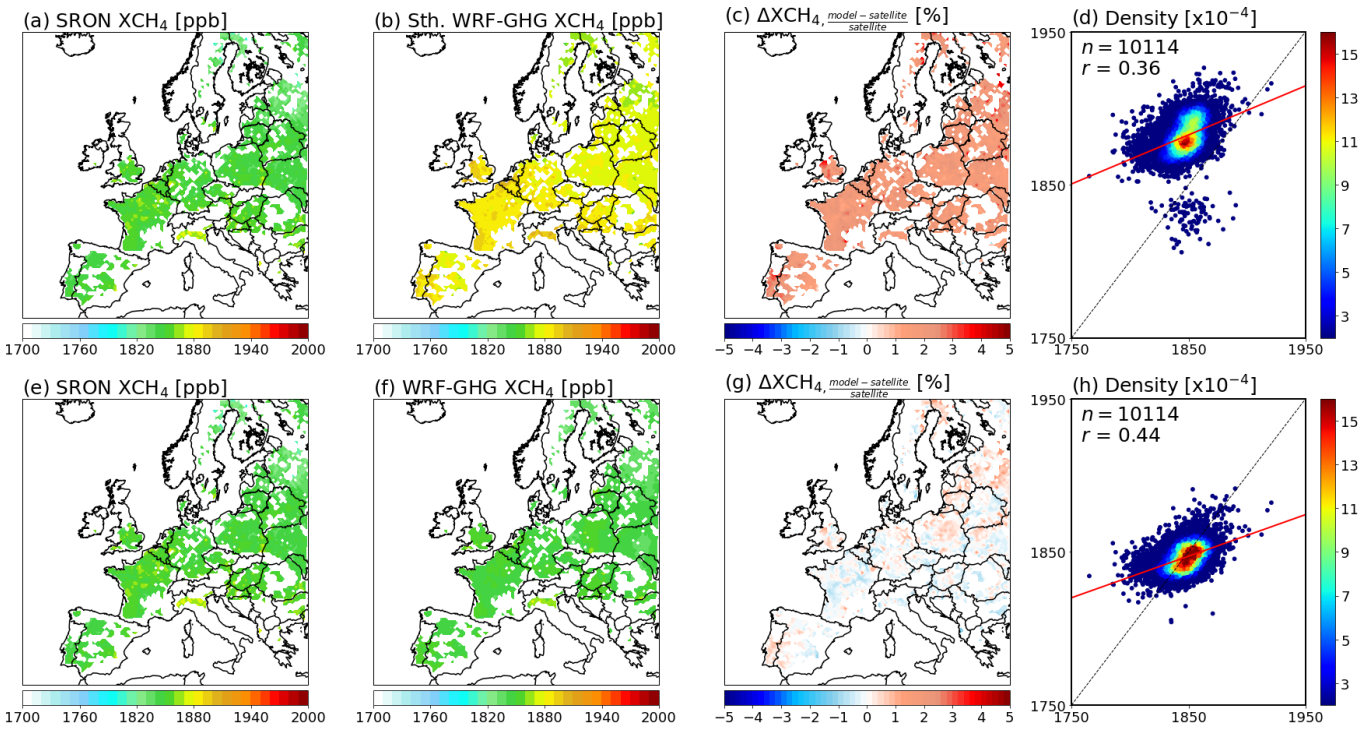

Figure S10. Temporal mean spatial distributions of XCH_4 concentration from SRON RemoTeC-S5P (panels a and e) and WRF-GHG estimates with and without smoothing (panels b and f, respectively), along with their relative differences (panels c and g), averaged over the period from September 1 to September 30, 2018.

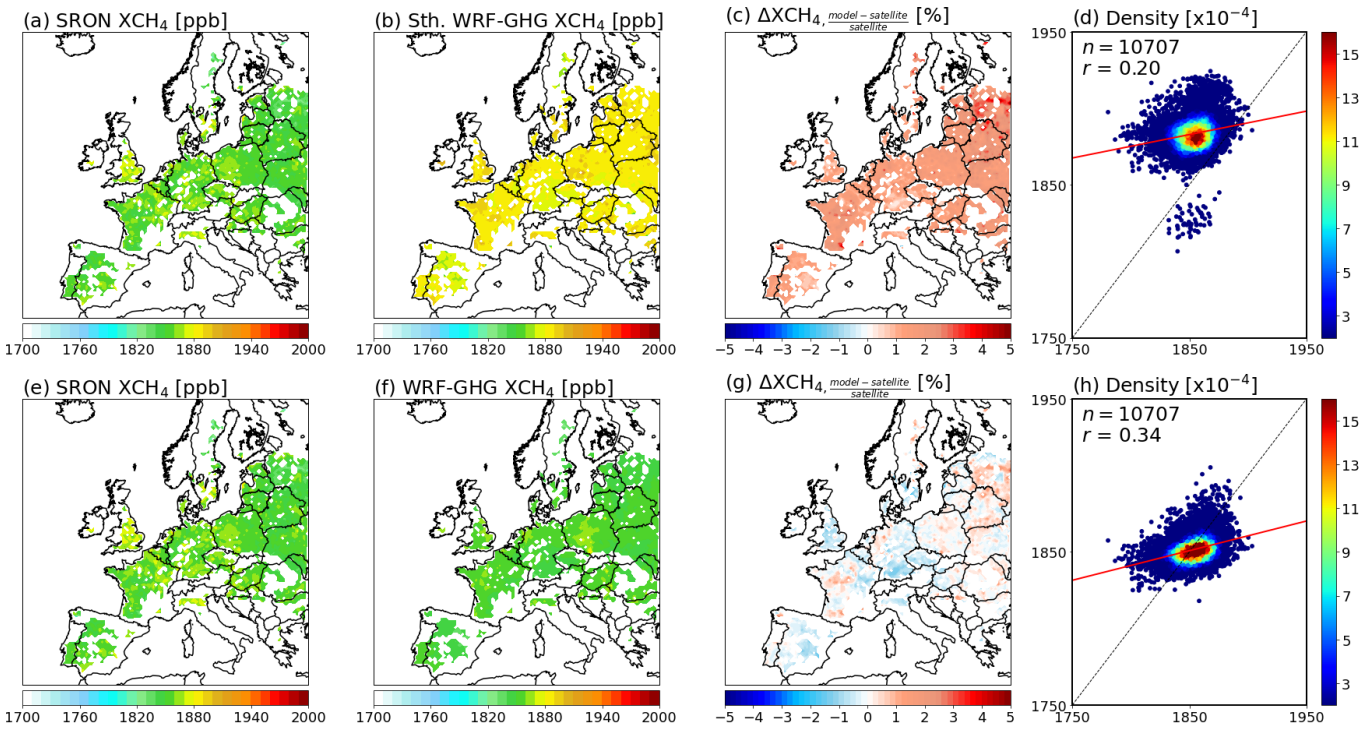

Figure S11. Temporal mean spatial distributions of XCH_4 concentration from SRON RemoTeC-S5P (panels a and e) and WRF-GHG estimates with and without smoothing (panels b and f, respectively), along with their relative differences (panels c and g), averaged over the period from October 1 to October 31, 2018.

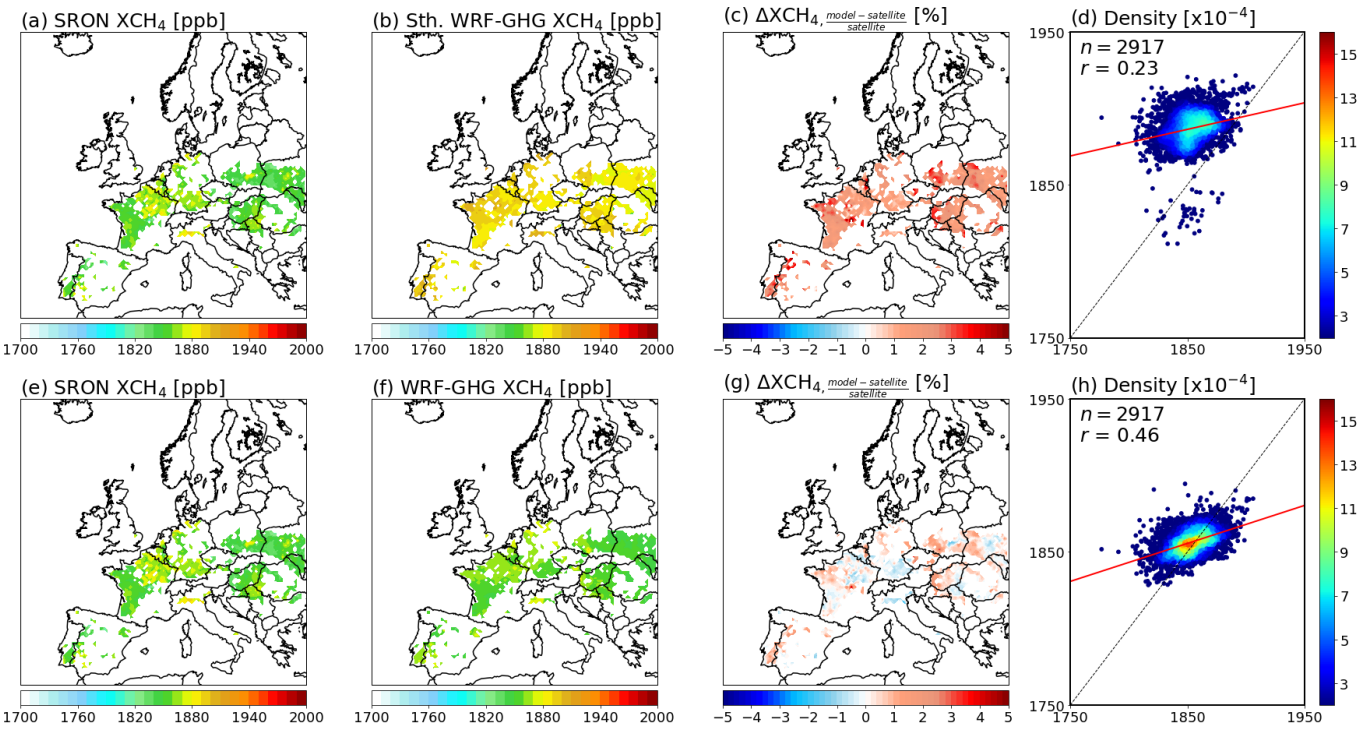

Figure S12. Temporal mean spatial distributions of XCH_4 concentration from SRON RemoTeC-S5P (panels a and e) and WRF-GHG estimates with and without smoothing (panels b and f, respectively), along with their relative differences (panels c and g), averaged over the period from November 1 to November 30, 2018.

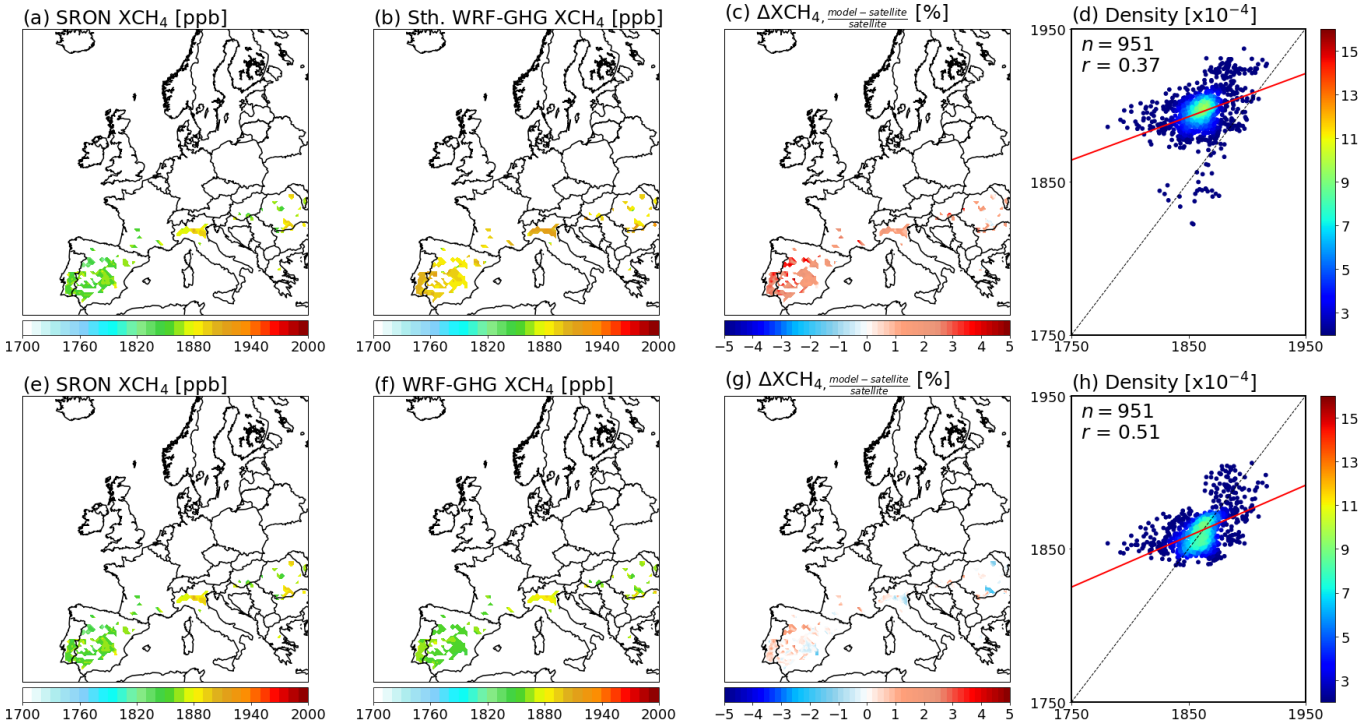

Figure S13. Temporal mean spatial distributions of XCH_4 concentration from SRON RemoTeC-S5P (panels a and e) and WRF-GHG estimates with and without smoothing (panels b and f, respectively), along with their relative differences (panels c and g), averaged over the period from December 1 to December 20, 2018.

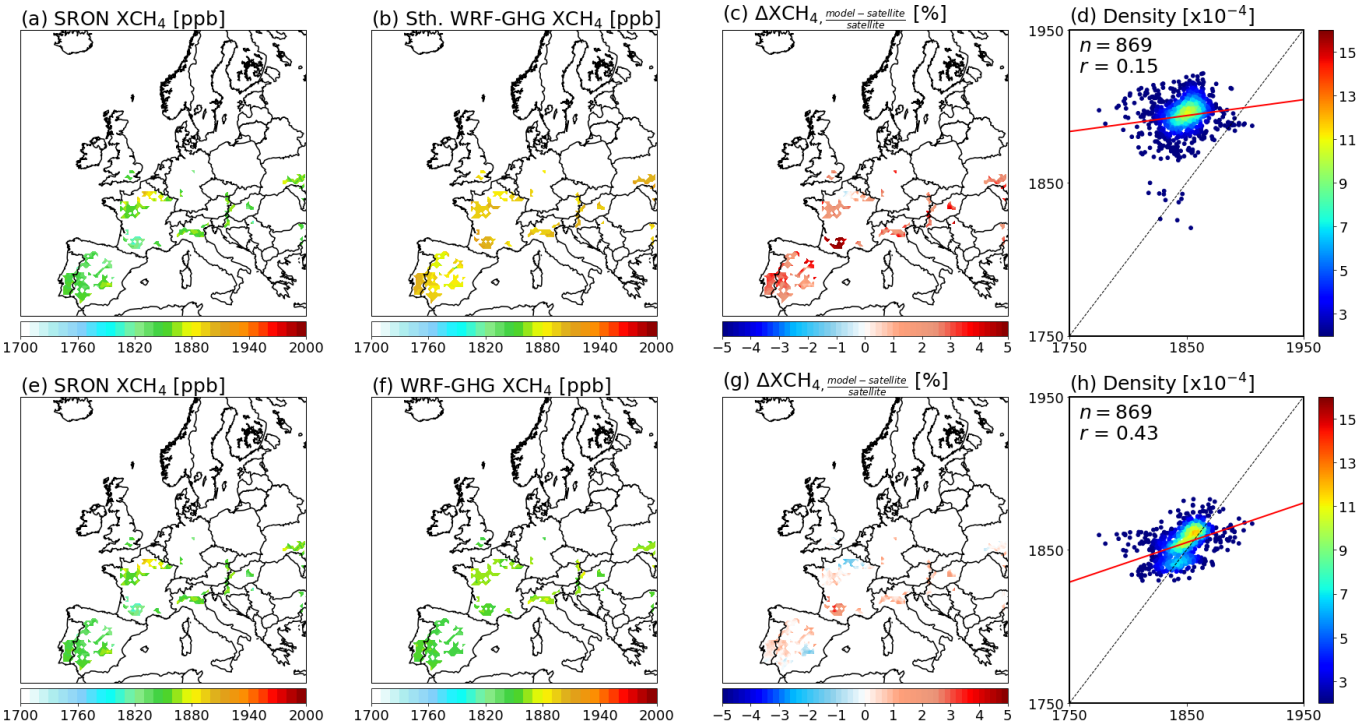

Figure S14. Temporal mean spatial distributions of XCH_4 concentration from SRON RemoTeC-S5P (panels a and e) and WRF-GHG estimates with and without smoothing (panels b and f, respectively), along with their relative differences (panels c and g), averaged over the period from January 15 to January 31, 2019.

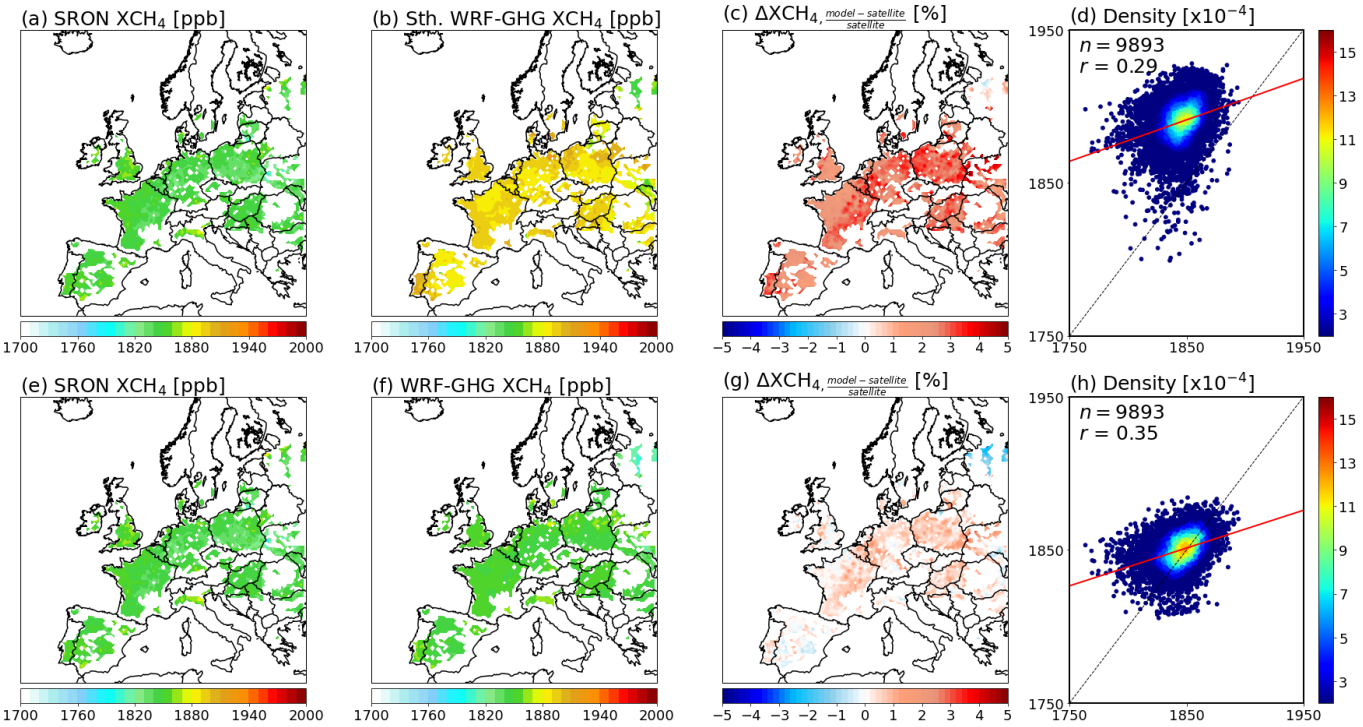

Figure S15. Temporal mean spatial distributions of XCH_4 concentration from SRON RemoTeC-S5P (panels a and e) and WRF-GHG estimates with and without smoothing (panels b and f, respectively), along with their relative differences (panels c and g), averaged over the period from February 1 to February 28, 2019.

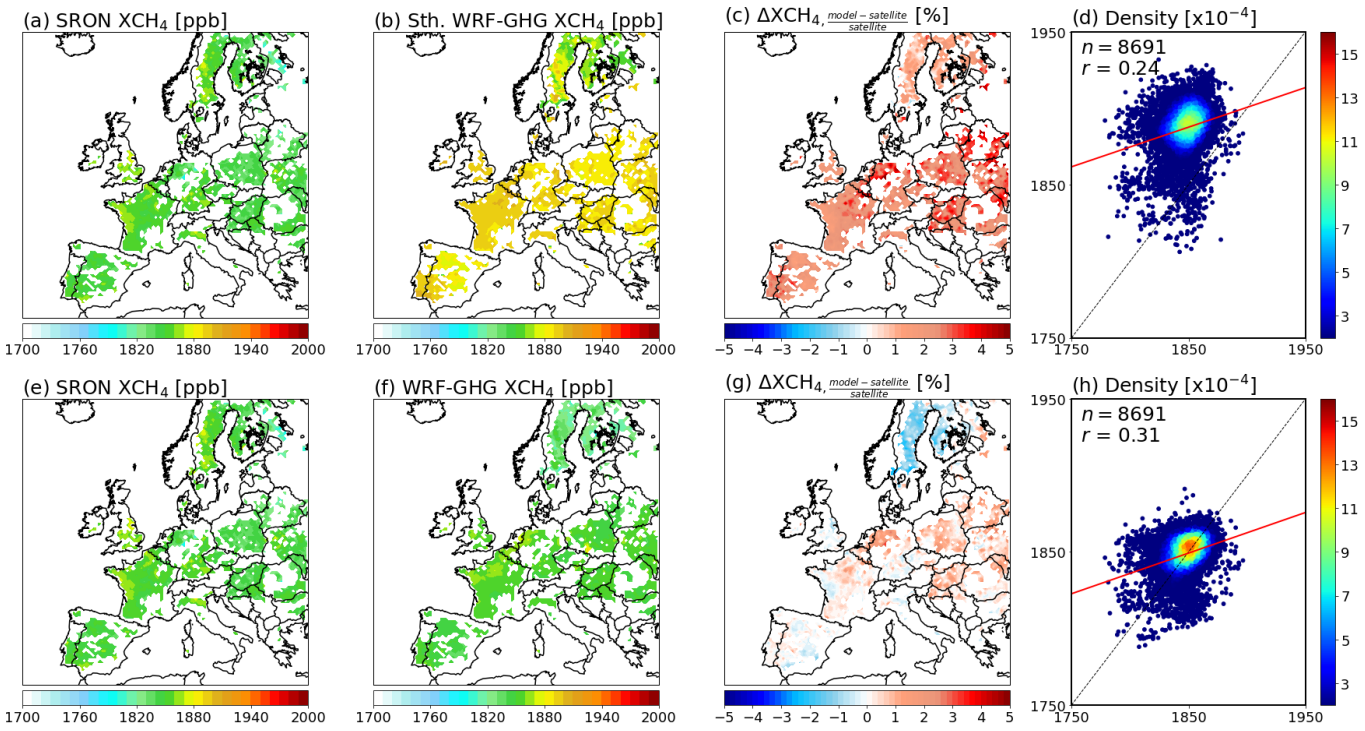

Figure S16. Temporal mean spatial distributions of XCH_4 concentration from SRON RemoTeC-S5P (panels a and e) and WRF-GHG estimates with and without smoothing (panels b and f, respectively), along with their relative differences (panels c and g), averaged over the period from March 1 to March 31, 2019.